RESEARCH ARTICLE

Macromolecular Rapid Communications
www.mrc-journal.de

Visualizing Penetration of Fluorescent Dye through Polymer Coatings

*Krishnaroop Chaudhuri, Riddhiman Medhi, Zhenglin Zhang, Zhuoyun Cai, Christopher K. Ober, and Jonathan T. Pham**

Understanding how small molecules penetrate and contaminate polymer films is of vital importance for developing protective coatings for a wide range of applications. To this end, rhodamine B fluorescent dye is visualized diffusing through polystyrene-polydimethylsiloxane block copolymer (BCP) coatings using confocal microscopy. The intensity of dye inside the coatings grows and decays non-monotonically, which is likely due to a combination of dye molecule transport occurring concurrently in different directions. An empirical fitting equation allows for comparing the contamination rates between copolymers, demonstrating that dye penetration is related to the chemical makeup and configuration of the BCPs. This work shows that confocal microscopy can be a useful tool to visualize the transport of a fluorophore in space and time through a coating.

1. Introduction

Polymer coatings are found in a variety of application areas, from food packaging[1–3] and automotive paints[4–8] to corrosion prevention[9–14] and material decontamination.[15–21] One of the primary functions of coatings is to protect the underlying substrate against external agents, such as solvents,[22–24] toxins,[25,26] bacteria,[27–32] or corrosive ions,[33–39] that are harmful to the underlying surface. Since these external agents vary, protective coatings need to be designed for the specific application in question. For example, silicone rubbers have low surface energy and low modulus, which can be beneficial for fouling release coatings.[40–43] On the other hand, silicones are often permeable to smaller molecules, like solvents or vapors;[44,45] this makes them useful for membranes but less useful for protection. For protecting surfaces from small molecules, mitigating penetration becomes important. Small molecule penetrants ultimately permeate most barriers over time, commonly known as a breakthrough time;[46,47] hence, it is important to understand what governs the kinetics of penetration and how to control it. One of the easiest examples to picture is protective rubber gloves. Gloves are used in laboratory settings but need to be removed when contaminated with solvents. Gloves act as a barrier, offering extra time for the user to remove the glove before solvents penetrate and contact the underlying skin.[48,49] Different materials (or gloves) provide different protection for different solvents, and hence it is useful to know how the chemical interactions relate to the penetration kinetics of small molecules in polymeric coatings.

To study penetration into polymer films and coatings, a range of different methods have been employed. Experimental techniques, such as permeation tests,[22,50] gravimetric studies,[51,52] and Taylor dispersion,[53] have been used to investigate the diffusion of solvents in polymeric systems. These methods often rely on periodically measuring the solvent uptake of the entire system or analyzing samples extracted as aliquots. Hence, the use of these techniques requires interruptions of the experiment or data collection being possible only at its conclusion. On the other hand, Varady et al. used FTIR as a method to continuously obtain concentration data of different components during the diffusion of a small molecule into a polymeric material.[54] While useful, this method of measuring the penetration rate does not provide clear spatial information about the diffusion process. One can imagine the situation of a drop splashing on a surface, where localized penetration of contaminants into the coating from the drop becomes important. However, characterizing this diffusion process is challenging with standard techniques.

K. Chaudhuri, J. T. Pham
Department of Chemical and Environmental Engineering
University of Cincinnati
Cincinnati, OH 45221, USA
E-mail: jonathan.pham@uc.edu

R. Medhi
Chemistry Department
University of Scranton
Scranton, PA 18510, USA

Z. Zhang, C. K. Ober
Department of Materials Science and Engineering
Cornell University
Ithaca, NY 14853, USA

Z. Cai
Department of Chemical and Materials Engineering
University of Kentucky
Lexington, KY 40506, USA

The ORCID identification number(s) for the author(s) of this article can be found under https://doi.org/10.1002/marc.202300304

DOI: 10.1002/marc.202300304

A common choice for visualizing different processes in polymers is through the use of fluorescent molecules (i.e., dyes). This has been employed to study transport processes relevant for drug delivery,[55] solvent diffusion,[48,56] aggregation,[57] biological tissues,[58,59] and wastewater treatment.[60,61] Fluorescent mechanophores have also been embedded into polymeric materials to understand the dynamics of crack propagation[62] or stress distributions.[63] Moreover, Hai et al. visualized the self-healing of hydrogels by measuring the real-time diffusion of fluorescent molecules across a breakage interface; however, this was on bulk samples placed side-by-side.[64] While all of these methods demonstrate the utility of fluorescent dyes in studying polymeric processes, they do not provide real-time analysis of penetration with spatial distributions through the depth of a thin film on microscopic size scales. For applications in protective coatings, a real-time method of visualizing the penetration of small molecules through the thickness, from a single contaminated drop, would be beneficial.

In this paper, we demonstrate the use of confocal microscopy as an approach to visualize how a fluorescent dye penetrates through the thickness of a polymer coating. Using image analysis, the fluorescence intensity inside the coating is tracked with respect to time and space through its depth. We derive an empirical model of dye penetration; this is then fit to our imaging data to obtain a contamination rate parameter, offering a semi-quantitative metric to compare penetration across different coatings. For the polymer, we employ a vinyl-modified polydimethylsiloxane (PDMS) and polystyrene (PS) block copolymer (BCP) system. Rhodamine B is used as our model fluorescent penetrant, which is known to penetrate into PDMS[65] but not PS.[66] This is likely due to favorable interactions between rhodamine B and PDMS, as well as the rubbery nature of PDMS chains at room temperature. On the other hand, PS is glassy at room temperature. This allows us to test the effect of PDMS content on penetration in different BCPs. Our method is able to illustrate differences in how dye penetrates into the coatings based on their material properties.

2. Results and Discussion

2.1. General Penetration Experiments

To prepare our samples for penetration experiments, PS-PDMS BCPs are dissolved in tetrahydrofuran (THF) at a weight ratio of ≈30% and spin-coated on glass to a thickness of ≈5 µm. The spin-coated samples are then placed on a confocal microscope equipped with a 40× objective (**Figure 1**). A 20 µL drop of dye solution (Rhodamine B in water at 20, 40, 80, or 160 µg g^{-1}) is then placed on the coating. Fluorescent, cross-sectional (*xz*-plane) images are then collected (Figure 1) at a rate of 0.571 s/frame. Due to the evaporation of water in the drop at prolonged times, the experiment is conducted for ≈15 min. For the polymer material, we synthesize PS-PDMS BCPs of varying PDMS to PS molecular weight ratios: Two diblocks (D) with a PS:PDMS weight ratio of 1:2.5 and 1:4.2 and one triblock (T) with a ratio of 1:5.0 (Figure 1b,c). Based on the block configuration and weight ratios, these are labeled as D-2.5, D-4.2, and T-5.0, respectively. The PDMS block is rubbery and offers flexibility due to its low glass transition,[67] whereas the PS block is stiffer and glassy,[68] acting

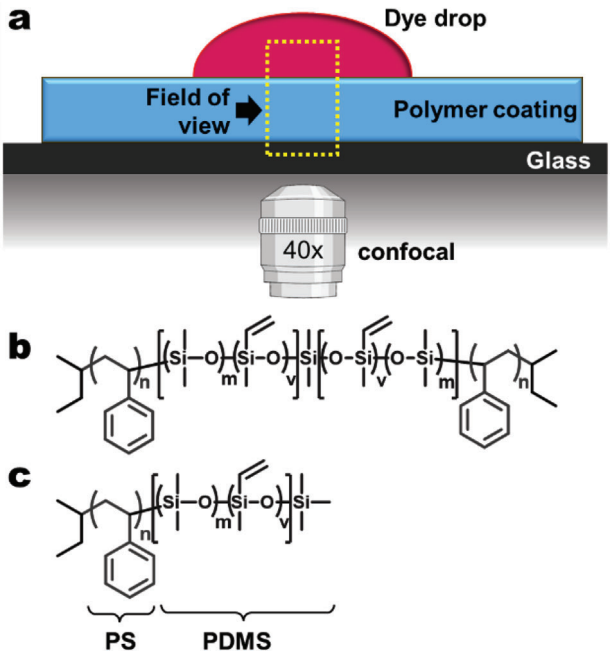

Figure 1. a) Schematic of the experimental setup for penetration tests through polymer coatings via confocal microscopy. A fluorescent dye drop is placed onto the coating while imaging via confocal microscopy. The yellow dotted box denotes the cross-sectional area of view in our microscope. The polymer structures include PS-PDMS block copolymers in b) triblock and c) diblock forms, where the number of vinylated (v) and number of non-vinylated (m) PDMS repeat units fall within 2–5 mole% vinylated, and *n* varies according to the PDMS:PS ratio. The vinyl groups are a small percentage and are assumed to play a negligible role compared to non-vinyl functionalized PDMS.

as physical crosslinks; such properties are beneficial for coatings applications. We note that there are some vinyl groups along the PDMS backbone, with the aim of modifying these polymers with different functionalities in future efforts. However, since the concentration of these vinyl groups is relatively small, we assume they do not behave much differently than PDMS without vinyl groups.

To describe our general methodology, we start by showing data from a 40 µg g^{-1} dye drop placed onto a T-5.0 coating. **Figure 2**a displays a sequence of images that show the movement of fluorescent dye through a coating, visualized in the *xz*-plane. We select 11 images out of a sequence of ≈700 to show the characteristic features of the dye penetration process. The video containing the entire sequence is provided in Video S1, Supporting Information. By comparing the thickness of the coating before and after the experiment, we confirm that no visible swelling occurs in the coating during the course of the experiment. Hence, the thickness can be considered to stay constant. At the moment of placing the drop, which is taken to be at time $t = 0$, no fluorescence is visualized inside the coating. As time progresses, an influx of dye into the coating is clearly observed. After $t \approx 16$ s, the dye front reaches the glass, where it starts to accumulate. This accumulation increases for ≈15 s, stabilizes briefly, and then fades until the glass interface has the same intensity as the rest of the coating. It should be noted that Rhodamine B can exhibit aggregation-induced quenching in solutions.[69] However, it is not observed

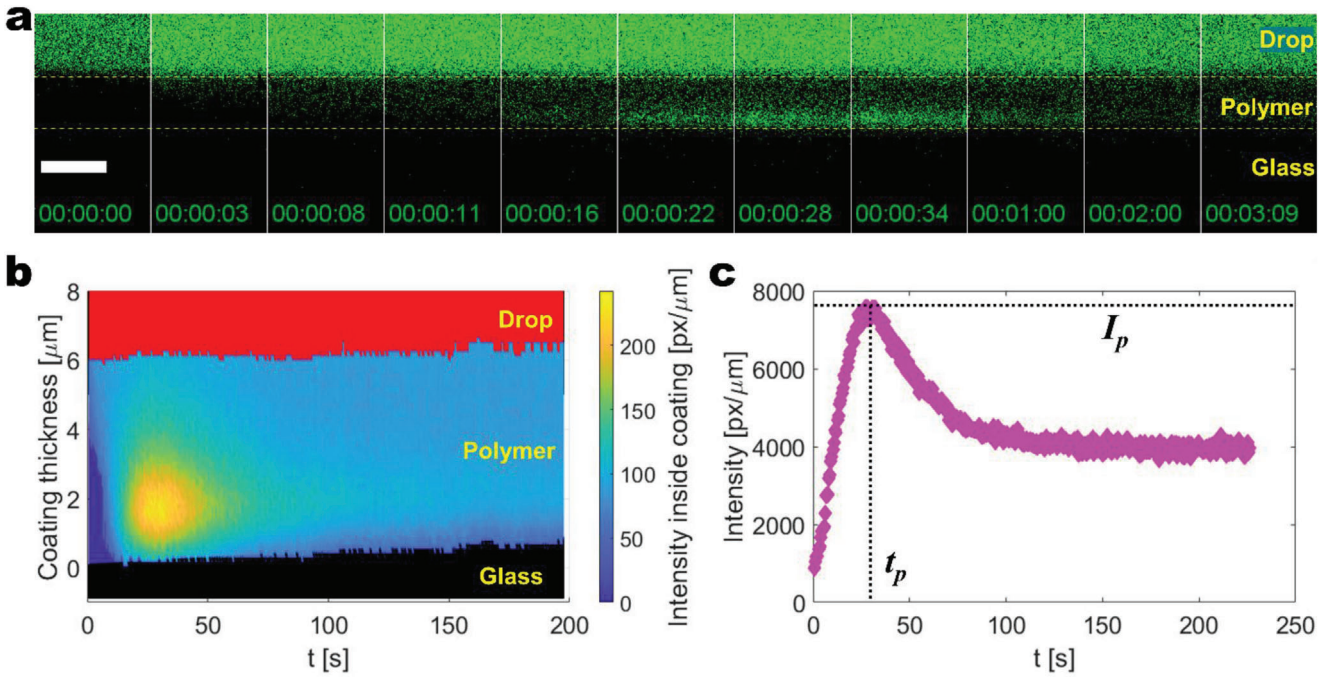

Figure 2. a) Sequence of snapshots taken from confocal microscopy imaging of 40 μg g^{-1} dye penetration in T-5.0. Scale bar: 10 μm. b) A spatio-temporal map of the intensity data obtained from the confocal images. The *x*-axis is the time-step and the *y*-axis represents the spatial distribution of dye in the coating at that time-step. The color indicates the intensity of the dye inside the coating according to the color bar. The drop (red) and glass (black) regions have been artificially colored and excluded from the calculations. c) Plot of intensity, normalized by the coating thickness, versus time obtained by the sum of intensities in the coating at each time-step. The time to peak t_p and local maximum peak I_p are labeled on the *x*- and *y*-axes, respectively.

within our coatings. Rhodamine B molecules have been shown to not self-quench at room temperature inside PDMS or other hydrophobic coatings.[70,71] To confirm, we performed control tests on a commercial PDMS elastomer and PS and found no observable reduction in the fluorescent intensity within the experimental timeframe of ≈15 min (Figure S1, Supporting Information). Moreover, these control experiments on PDMS-only and PS-only films confirm that Rhodamine B penetrates into PDMS and not PS (Figure S1, Supporting Information).

After each image of a video is analyzed, we obtain a 3D plot that provides spatiotemporal information on dye intensity (Figure 2b). Each time step in the *x*-axis shows the distribution of dye at that instant throughout the thickness (*y*-axis) of the sample. The color bar represents the fluorescence intensity at that point in time and space. The drop and glass are artificially colored to distinguish them from the coating and are excluded in subsequent calculations. In comparison to the confocal image sequence (Figure 2a), the surface plot in Figure 2b accurately represents the dye penetration dynamics. The coating is not fully pervaded by the dye in the first ≈10 s, illustrated by the zero intensity in the 0–4 μm region. After ≈10 s, the dye reaches the glass and builds up in the 0.5–3 μm region between 20 and 60 s (yellow zone). Following confocal observations, this bright region vanishes and the entire coating has a uniform intensity for the remainder of the experiment.

We obtain a sum total change of dye intensity over time by integrating the surface plot over the thickness (Figure 2c). While this integration loses spatial information of fluorescence across the thickness, these 2D graphs provide a simple measure of dye inside the coating over time. The integration captures a rapid rise of dye intensity in the first ≈30 s, which peaks, followed by a drop in intensity and then an approximate stabilization. The time it takes for the intensity to reach the local maximum peak (I_p), after the rapid rise, will be termed the time to peak (t_p).

To explain the non-monotonic shape of the intensity versus time curve, we hypothesize that fast penetration occurs through the thickness of the coating and a slower process occurs outward from our field of view (**Figure 3**a). When the dye drop is placed on the surface, rapid penetration occurs through the thickness of the coating (P1, Figure 3a); this is a short, micron-scale distance. Once the dye reaches the glass, it begins to accumulate inside the entire bulk of the coating. This accumulation causes the intensity peak (I_p). Since there is a large region of the coating that is away from the drop, a chemical potential drives dye from the penetrated region directly under the drop to the clean regions away from the drop. This transport process (P2) is slower than that in the direction through the thickness (P1). This is because: i) the concentration difference of dye per unit volume between the liquid drop and the coating (P1) is much larger than that between the contaminated and clean regions of the coating (P2), and ii) the lateral diffusion P2 has to traverse over a much larger distance. To test this hypothesis, we visualize the velocity of the dye front for a T-5.0 sample with a dye concentration of 80 μg g^{-1} from two viewpoints. One is the downward moving front (P1, Video S2a, Supporting Information) and the other is the laterally moving front away from the edge of the dye drop (P2, Video S2b, Supporting Information). To compare the velocities, we plot the front displacement as a function of time and take the

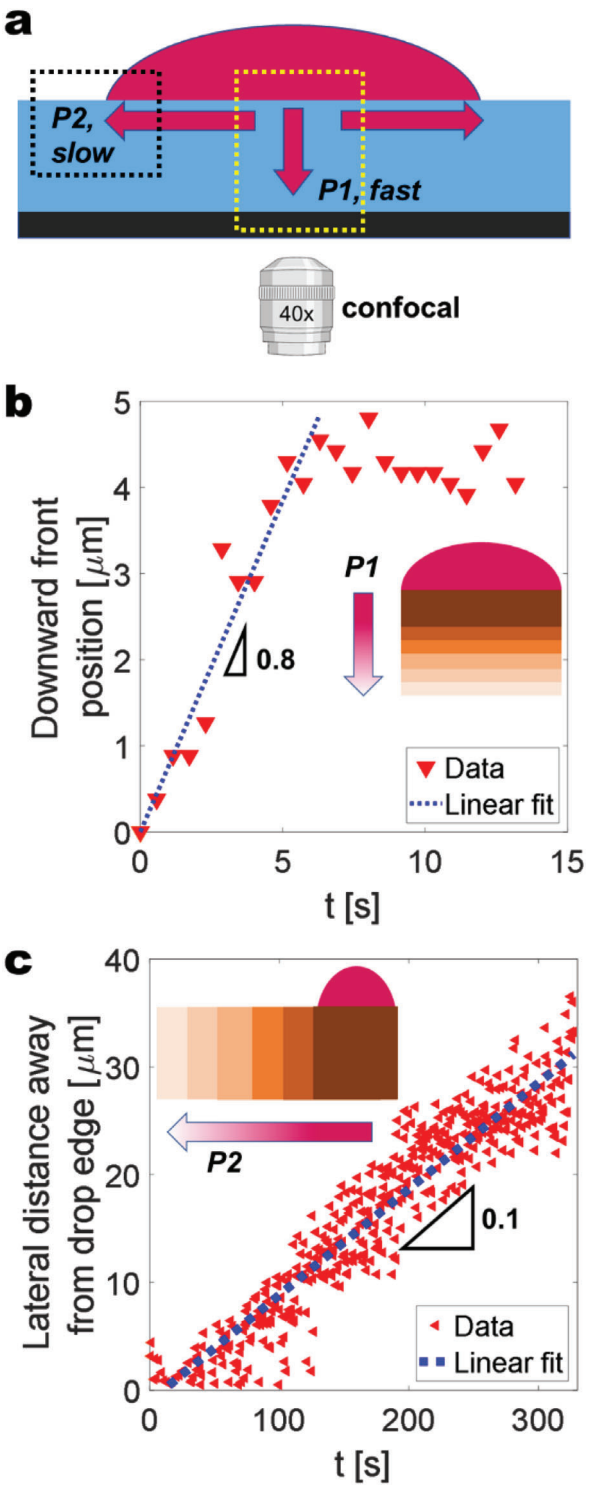

Figure 3. a) Schematic of the proposed mechanism of dye transport from the drop (red) to the coating (blue). The fast process P1 is through the thickness while the slow process P2 is lateral. The displacement of the dye front (red triangles) and its slope (blue dotted lines) is measured b) downward, P1, and c) laterally, P2, using a T-5.0 coating with an 80 μg g^{-1} dye drop. The yellow and black dotted lines indicate the imaging area in confocal view for processes P1 and P2, respectively. Fewer data points exist for the downward slope in (b) because there are fewer frames captured within the <10 s for the dye to reach the glass.

slopes (Figure 3b,c). Consistent with our hypothesis, the velocity through the thickness is ≈8× faster than the lateral velocity. Although P2 begins after P1, it is likely that both processes occur simultaneously after a short period, with P2 dominating over P1. It should be noted that the start of process P2 does not imply that the coating is saturated with dye; dye is still accumulating inside the bulk of the coating, while also being transported away to cleaner parts of the coating.

2.2. Comparison of Block Copolymers

Having established the methods for interpreting confocal data, we consider differences in penetration between our three BCPs. Although the primary focus of this paper is to visualize the localized transport of contaminants through polymer coatings from a contaminated drop, we expect that the penetration behavior will differ as a function of the different BCP materials. Several aspects of the penetration data can be used to make a comparison including i) the time it takes to reach the peak point (t_p), where process P2 starts to become relevant, ii) the height of this peak itself (I_p), and iii) the general trends observed for each BCP as a function of dye concentration. To make a comparison between the three BCPs while keeping a constant dye concentration, we plot intensity versus time for the lowest (20 μg g^{-1}) and highest (160 μg g^{-1}) concentration dye solutions (**Figure 4**a,b). For the 20 μg g^{-1} case, the D-2.5 shows the highest integrated intensity peak (I_p), as well as the longest time to the peak (t_p). For D-4.2, the peak becomes difficult to see, although a zoom-in of this data indeed shows a local maximum, which we will consider as a peak. For the T-5.0, we find an intermediate I_p and t_p that lies between the D-2.5 and D-4.2. For the 160 μg g^{-1} case, we see the same general trend, but with different absolute values. We initially hypothesized that higher PDMS content in the BCPs would lead to higher penetration rates, which would manifest through shorter times to peak, t_p. We emphasize here that higher I_p does not necessarily mean higher penetration rates, but actually the opposite. This is because the dye penetrates through the coating thickness (P1) and accumulates dye, while only slowly migrating laterally out of our field of view (P2). Indeed, we find that the PDMS content in diblock copolymers follows this hypothesis, where D-2.5 has a higher I_p and t_p than D-4.2; however, the T-5.0 does not fit this trend. Hence, our results suggest that the polymer configurations may play a role in the penetration behavior.

To gain insight into the effect of dye concentration within each BCP type, we present their intensity versus time data in separate graphs (Figure 4c–e). For both D-2.5 and T-5.0 BCPs, we find that both I_p and t_p increase with decreasing dye concentration. In these cases, lower dye concentration leads to slower penetration (higher t_p) through the thickness (P1), which then accumulates dye and increases intensity (I_p). Whereas for higher concentrations, the dye penetrates into the coating quicker due to a greater chemical potential difference between the dye-rich water drop and the dye-deficient polymer coating. The dye is then rapidly transported laterally (P2), leading to less accumulation within the region immediately beneath the drop and within our imaging region. In other words, since the driving force of dye penetration increases with concentration, the resultant faster kinetics leads to lower t_p. In contrast to D-2.5 and T-5.0, I_p decreases

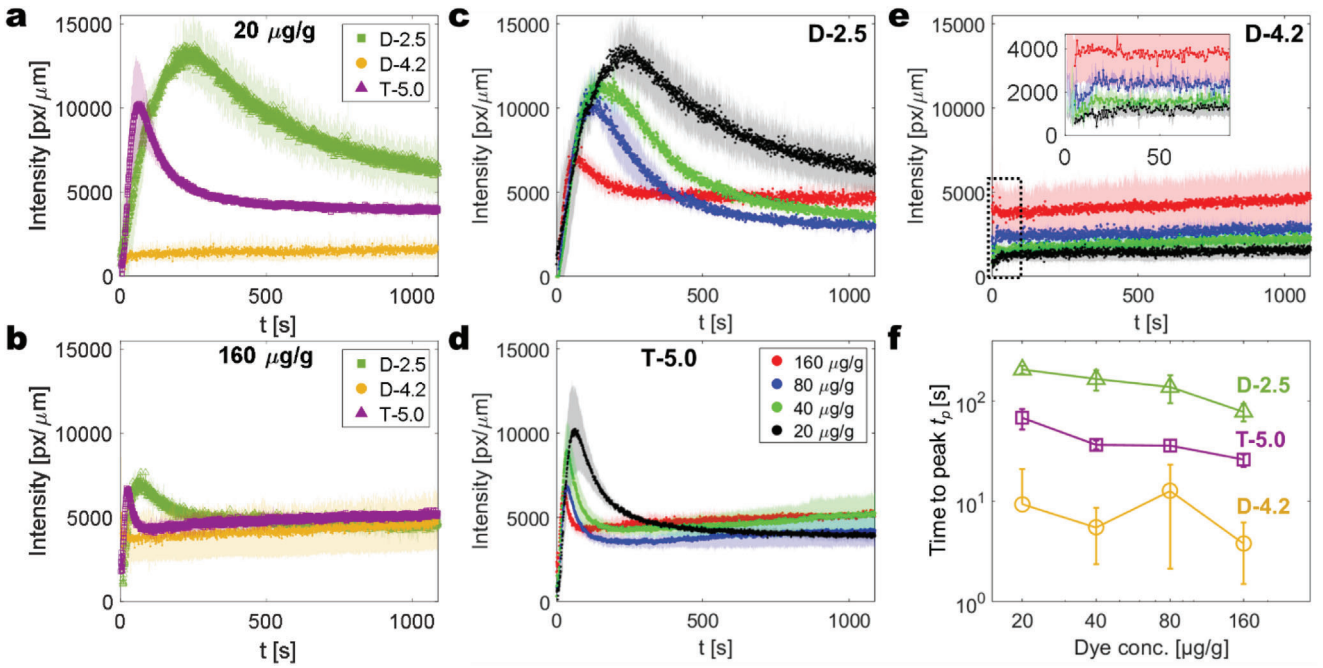

Figure 4. Intensity versus time data for all block copolymers for dye concentrations a) 20 μg g^{-1}, and b) 160 μg g^{-1}. Intensity versus time for block copolymers c) D-2.5, d) T-5.0, and e) D-4.2 with varying dye concentrations. The inset in (e) shows the peak point in the first minute. The shaded area represents error over three data sets. f) Time to peak versus dye concentration for all three block copolymers. Error bars represent the standard deviation over three data sets.

with decreasing dye concentration for the D-4.2, while t_p remains roughly constant. This suggests that the penetration occurs very rapidly, where process P1 is almost negligible and the transport may be approaching a steady state; that is, dye moves from the drop through the coating thickness and then laterally at the same rate. As an overview, a plot of t_p as a function of dye concentration for the different BCPs is presented in Figure 4f.

The penetration of a coating from a small drop of liquid is complex since there are two concurrent transport processes due to the thin geometry of the coating. Hence, the penetration process imaged within our field of view cannot be quantified with traditional diffusion. In an attempt to make a semi-quantitative comparison of penetration between BCPs, we propose the following empirical equation, which accounts for the two transport directions. This simplified model assumes that i) the accumulation process (which is the influx of dye from the drop into the coating region immediately underneath it) follows zero-order kinetics, and that ii) the lateral migration (from the region of the coating in contact with the drop to other uncontaminated regions) is a first-order process. At any given time t, the fluorescence intensity inside the coating $F(t)$ can be expressed as

$$F(t) = F_0 + \left(r_0 t - F_0\right) e^{-pt} + r_\infty t \tag{1}$$

where r_0 is the rate at which dye accumulates inside the coating underneath the drop, and p is the rate at which it is migrating to uncontaminated regions of the coating. F_0 (with units of intensity) can be considered as the intensity left in the coating under the drop after the peak has decayed. Whether the intensity $F(t)$ is a constant F_0 or slowly increasing, depends on the term r_∞, which is associated with the slope of the line at long times. For D-2.5, $r_\infty \to 0$ and $F(t) \approx F_0$ is the approximately constant value of the intensity inside the coating after the peak has decayed. The unit of p is s^{-1} while r_0 and r_∞ have units of intensity/time. Similar models have been used for analogous systems, such as drug delivery in kidneys.[72,73]

Since the processes P1 and P2 have a combined influence on the rates r_0 and p, either quantity cannot be chosen as the sole variable representing the rate of dye moving through our imaging region. Additionally, the post-decay intensity is important to quantify the level of contamination in a coating. Hence, we define a term K_c indicating the "contamination rate" as

$$K_c \equiv \frac{F_0 p}{r_0} \tag{2}$$

This quantity includes parameters in the exponential part of Equation (1), which describes the non-monotonic shape of the intensity profiles. It scales as the ratio of the lateral migration rate p relative to the accumulation rate beneath the drop r_0. A higher value of F_0 implies that more dye is left after the decay, indicating a higher degree of contamination. Moreover, multiplying by F_0 makes the term dimensionless for comparison. Hence, K_c is an empirical metric that can be used to represent the rate at which dye passes through the bulk of the coating, where a higher K_c represents a higher contamination rate.

Equation (1) is a parametric equation that we fit to the experimental data without any a priori information. As an example, an overlay of Equation (1) fit to data of an 80 μg g^{-1} dye drop demonstrates a reasonably good fit (**Figure 5**a); the equation effectively captures the peak, decay, and possible slow increase in long times, albeit with fitting parameters. For K_c, we find an

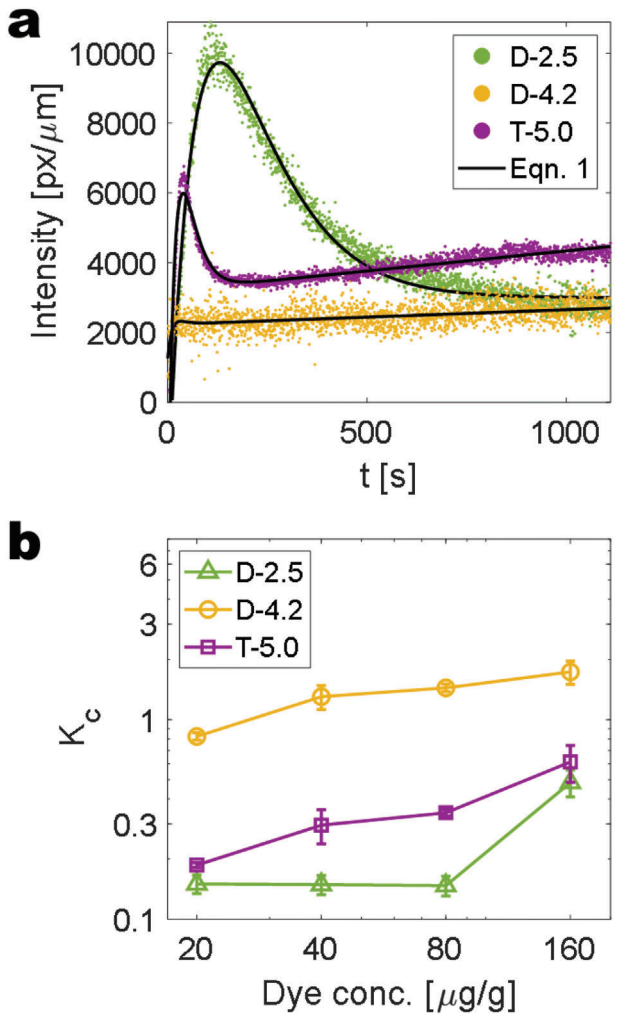

Figure 5. a) Representative data (dots) of three block copolymers with 80 μg g^{-1} dye penetration, overlaid by a fit of Equation (1) (line). b) Rate of contamination parameter K_c (Equation (2)) versus dye concentration for the three-block copolymers. Error bars represent the standard deviation over three data sets.

increase with increasing dye concentration for our three BCPs (Figure 5b). This may be intuitive since a larger dye concentration has a larger driving force for penetration and contamination. For the two diblocks, the contamination rate K_c increases with increasing PDMS content as expected (i.e., D-4.2 is higher than D-2.5). However, we again find that despite T-5.0 having the highest PDMS content, it has an intermediate value for K_c. Hence, this continues to suggest that the block configuration plays a role in the dye contamination behavior.

Based on our knowledge that Rhodamine B penetrates PDMS while it does not visibility penetrate PS, we initially hypothesized that the contamination rates K_c would be solely governed by the PDMS content. However, our results suggest a different trend. It is possible that the different polymer structures lead to different transport properties. Due to incompatibilities between the PS and PDMS blocks, the blocks segregate from one another. The diblocks and triblocks would likely form different assembled structures. The diblocks may form lamellar structures with alternating microdomains or micellular-like structures with a PS aggregate surrounded by a PDMS matrix with free chain ends (**Figure 6**a). In this case, dye molecules have more available space to move through the flexible PDMS regions, since chain ends can be associated with more free volume. On the other hand, the triblock has PS end blocks, which may form a more traditional, elastomeric structure. The PS chains aggregate to form crosslinking sites between a PDMS chain, where the PDMS chain can act as a bridge between PS cores or form loops (Figure 6b). In this triblock case, the path is likely more hindered because the PDMS chains are tethered on both sides without free floating chain ends. Prior literature indeed suggests the microstructure of the coatings would differ from each other. Chen et al. observed diblock and triblock PS-PDMS films using TEM,[74] which incidentally have similar PS:PDMS ratios as ours. These BCPs exhibited parallelly oriented lamellar microdomains near the free surface and randomly oriented microdomains in the bulk. The only apparent difference between the diblock and the triblock copolymers is in their lamellar periodic lengths, which are ≈60 and 45 nm, respectively. This may indicate that the smaller structural domains in triblock copolymers result in a reduction in penetration rate by hindering dye molecule mobility, compared to the diblock copolymers; this is consistent with our findings. It is also consistent with the idea that free chain ends lead to larger PDMS regions. However, their study included thermal annealing which was not conducted here. On the other hand, O'Driscoll et al. found different microstructures, depending on the coating thickness, annealing process, or underlying substrate for PS-PDMS copolymers;[75] such parameters are outside the scope of the current effort. Although it still needs validation, based on current literature, this suggested molecular picture may offer a few reasons why K_c is lower for T-5.0 compared to D-4.2, despite having a larger PDMS content.

3. Conclusion

We demonstrate the use of confocal microscopy as a potential tool for visualizing the penetration and contamination of a polymer coating with a fluorescent dye. We used varying concentrations of Rhodamine B in water on PS-PDMS BCPs with different configurations. The intensity of dye that penetrates into the coating increases rapidly, reaches a peak, and then decays. This non-monotonic behavior in intensity likely arises from two dye transport processes occurring in different directions during the contamination process. A faster process occurs through the thickness of the coating, resulting in the influx and accumulation of dye. A slower process occurs laterally and is responsible for dye moving to uncontaminated regions of the coating. We use an empirical parameter K_c to compare contamination rates between BCPs. K_c increases with PDMS content when comparing diblocks; however, the triblock does not follow the same trend. This unexpected trend may result from different ways the polymer chains organize into structures. Future efforts may wish to consider the effect of annealing and molecular organization on the contamination rates. We hope that this work is useful for the development of protective paints, films, and coatings, as well as for enriching our understanding of diffusion in polymers.

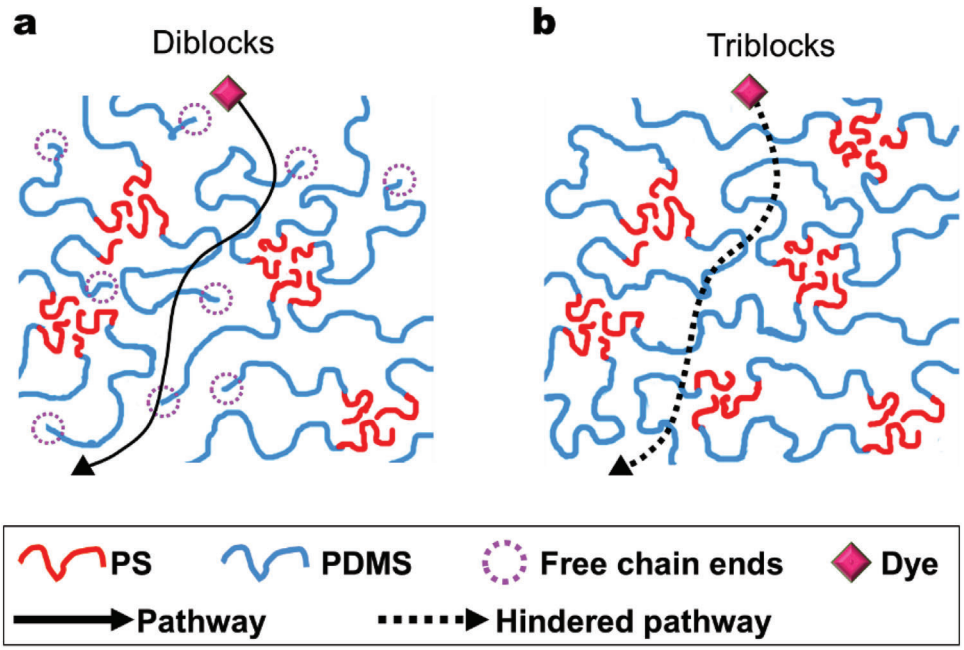

Figure 6. A possible molecular-scale picture of how the block configuration may affect the penetration of the dye. The a) diblocks may have a less hindered pathway for dye motion than the b) triblock due to the effects of free chain ends.

4. Experimental Section

Materials: All chemicals were purchased from Sigma Aldrich and solvents from VWR and used as received unless specified otherwise. Hexamethylcyclotrisiloxane (D3) and 1,3,5-trivinyl-1,3,5-trimethylcyclotrisiloxane (V3) were purchased from Gelest, Inc. Rhodamine B dye (Merck KGaA) solution was prepared with DI water (VWR International) to concentrations of 20, 40, 80, and 160 μg g^{-1}. Benzene was stirred over *n*-butyl lithium and diphenylethylene, distilled, and freeze-pump-thawed to degas. Styrene was dried over calcium hydride, distilled, and free-pump-thawed to degas. D3 was dissolved in benzene and stirred over calcium hydride for 24 h at which point a living anionic styrene polymerization was added and allowed to stir until the orange color had completely disappeared. The benzene was subsequently distilled, and the D3 sublimed, and then the solution was freeze-pump-thawed to degas. Solution concentration was determined using nuclear magnetic resonance spectroscopy (NMR). THF was stirred over calcium hydride and distilled into a flask containing sodium and benzophenone, and allowed to stir for several days, at which point it was distilled and freeze-pump-thawed to degas. V3 was stirred over calcium hydride, distilled, and freeze-pump-thawed to degas.

PS-PDMS Polymer Synthesis: PS-PDMS polymers were prepared exactly according to a previously reported method.[43,76] In brief, in a glovebox sec-butyl lithium was added to a flask charged with benzene and a stir bar, followed by the dropwise addition of styrene, leading to the development of a deep orange color. The reaction progressed overnight before sampling, followed by the addition of a solution of D3 in benzene. After the complete disappearance of the orange color, indicative of the live styrene anion, THF was added and the reaction was allowed to continue for 2 h. At this point, the addition of a solution of V3 in THF by syringe pump was begun and allowed to progress over 48 h. After addition, the polymerization was allowed to react for an additional 24 h. The polymerization was end-capped with chlorotrimethylsilane for the formation of diblock, and with a solution of dichlorodimethylsilane in THF for the triblock (adding 75% of the dichlorodimethylsilane directly, followed by the addition of the remaining 25% of dichlorodimethylsilane by syringe pump over a 24-h period). Polymers were precipitated directly into a 4/1 (v/v) mixture of methanol and deionized water and allowed to stir overnight. Polymers were collected by vacuum filtration and dried overnight in a vacuum oven at 55 °C.

Sample Preparation: Glass coverslips of thickness ≈0.15 mm used as substrates for the coatings were thoroughly cleaned by sonication using soap solution, DI water, and ethanol for 45 min each. These substrates were dried and treated for 30 min in a UV-Ozone chamber prior to film casting. The BCP samples were dissolved in THF (Avantor, Inc.) for 24 h at a polymer concentration of ≈30% by weight. These viscous solutions were spin-coated onto the centers of glass slides. To have sufficient *z*-axis distance for visualization, as well as to minimize image aberration, the film thickness was kept to ≈5 μm; hence, spin coating speeds were varied between 500 and 800 rpm to account for the different viscosities and drying rates of the solutions. The different viscosities arise due to the differences in molecular weights of the different polymers. The spin coating duration and polymer solution drop volume were kept constant at 2 min and 20 μL, respectively. It should be noted that efforts to keep the thickness of the coatings constant at around 5 μm were made, however, due to the high solids and viscosity, combined with small sample volume and volatile solvent, small amounts of evaporation led to some variations.

Confocal Microscopy: The clean films were loaded on a confocal microscope (Leica SP8) with a 40× objective equipped with a piezo controller. At time $t = 0$, a dyed drop of volume 20 μL was placed on the focused region of the coating such that the drop-coating-glass layers were clearly visible in the imaging window in the *xz*-plane. The images were recorded continuously at the rate of 0.571 s/frame. Usually, the experiment was stopped after ≈15 min following which evaporation may have stronger effects on the dye concentration of the drop.

Image Processing: The raw image data obtained as grayscale images were used to measure the movement of fluorescent dye inside the coating both spatially and temporally. Due to changes in the intensity of fluorescence in the drop and coating layers, and its absence in the glass, these three regions could be easily demarcated for all images. The intensity values of the pixels can be considered to be directly correlated to the amount of fluorescent dye in that region. For all images, the background noise was deleted using the pixel intensity of the glass region as a reference. The fluorescence inside the coating was measured by integrating over the *x*-axis, which was along the horizontal direction of the sample. Hence for each time step, the profile of the intensity variation was obtained along the *z*-axis (direction of the thickness of the coating) as a 3D surface plot. This enabled to visualize how the dye localizes inside the thickness of the

coating over time. The image processing method also accounted for the fact that the sample might shift on the confocal microscope, either during drop loading or over time due to external vibrations. To measure the total amount of dye inside the coating at any given point of time, this 3D surface plot was further integrated along the *z*-axis and obtained a line graph as seen in Figure 2c. These plots enabled to quantitatively compare the dye penetration dynamics across the different BCPs and dye concentrations. While care was taken to ensure comparable sample thickness throughout all samples, there were small variations in the thicknesses of the coatings. Hence all integrated pixel values for the 2D plots were normalized by the corresponding sample thickness; the units of intensity in this paper are reported as pixels/μm.

Supporting Information

Supporting Information is available from the Wiley Online Library or from the author.

Acknowledgements

The authors thank Anthony Malanoski and Brandy White from the Naval Research Laboratory (NRL) for helpful discussions. This work was supported financially by the Defense Threat Reduction Agency (DTRA), contract number RD-CBT PS1BR-CB10828, via NRL contracts N00173-22-2-C001 and N00173-22-2-C003.

Conflict of Interest

The authors declare no conflict of interest.

Data Availability Statement

The data that support the findings of this study are available from the corresponding author upon reasonable request.

Keywords

confocal microscopy, contamination, penetration, polymeric coatings

Received: June 23, 2023
Published online:

[1] S. Mangaraj, A. Yadav, L. M. Bal, S. K. Dash, N. K. Mahanti, *J. Packag. Technol. Res.* **2019**, *3*, 77.
[2] T. Huang, Y. Qian, J. Wei, C. Zhou, *Polymers* **2019**, *11*, 560.
[3] S. Sid, R. S. Mor, A. Kishore, V. S. Sharanagat, *Trends Food Sci. Technol.* **2021**, *115*, 87.
[4] L. Lin, G. S. Blackman, R. R. Matheson, *Prog. Org. Coat.* **2000**, *40*, 85.
[5] A. Kausar, *J. Macromol. Sci., Part A: Pure Appl. Chem.* **2018**, *55*, 440.
[6] G.i Y. Kim, S. Sung, M. P. Kim, S. C. Kim, S.-H.o Lee, Y. I.l Park, S. M. Noh, I.n W. Cheong, J. C. Kim, *Appl. Surf. Sci.* **2020**, *505*, 144546.
[7] P. G. Wagle, S. S. Tamboli, A. P. More, *Prog. Org. Coat.* **2021**, *150*, 106005.
[8] J.i H. Jeong, J. Seo, M. Kim, C. Park, H. J. Kim, Y. H. Choi, H. Kim, Y. Eom, *Prog. Org. Coat.* **2023**, *177*, 107412.
[9] A. Stankiewicz, I. Szczygiel, B. Szczygiel, *J. Mater. Sci.* **2013**, *48*, 8041.
[10] L.i Cheng, H. Wu, J. Li, H. Zhao, L. Wang, *Corros. Sci.* **2021**, *178*, 109064.
[11] A. Trentin, A. Pakseresht, A. Duran, Y. Castro, D. Galusek, *Polymers* **2022**, *14*, 2306.
[12] C. I. Idumah, C. M. Obele, E. O. Emmanuel, A. Hassan, *Surf. Interfaces* **2020**, *21*, 100734.
[13] A. Kausar, *J. Plast. Film Sheeting* **2020**, *36*, 391.
[14] M. Faccini, L. Bautista, L. Soldi, A. M. Escobar, M. Altavilla, M. Calvet, A. Domènech, E. Domínguez, *Appl. Sci.* **2021**, *11*, 3446.
[15] H.-M. Yang, C. W. Park, K.-W. Lee, *Prog. Nucl. Energy* **2018**, *104*, 67.
[16] H. N. Gray, B. Jorgensen, D. L. Mcclaugherty, A. Kippenberger, *Ind. Eng. Chem. Res.* **2001**, *40*, 3540.
[17] Y. Xue, W. Yang, R. Yue, Y. Chen, *Polymers* **2022**, *14*, 1656.
[18] A. Gossard, A. Lilin, S. Faure, *Prog. Nucl. Energy* **2022**, *149*, 104255.
[19] S. V. S. Rao, K. B. Lal, *J. Radioanal. Nucl. Chem.* **2004**, *260*, 35.
[20] G. Toader, P.-O. Stanescu, T. Zecheru, T. Rotariu, A. El-Ghayoury, M. Teodorescu, *Arabian J. Chem.* **2019**, *12*, 4026.
[21] G. Toader, D. Pulpea, A. Diacon, E. Rusen, R. E. Ginghina, T. Rotariu, A. I. Podaru, A. E. Moldovan, M. Gavrilescu, A.-M. Gavrila, B. Trica, *Water* **2023**, *15*, 982.
[22] K.-P. Chao, P. Wang, Y.a-T. Wang, *J. Hazard. Mater.* **2007**, *142*, 227.
[23] P. I. Dolez, T. Vu-Khanh, *Int. J. Occup. Saf. Ergon.* **2009**, *15*, 347.
[24] S. Xiao, C. Moresoli, A. Burczyk, P. Pintauro, D. D.e Kee, *J. Environ. Eng.* **1999**, *125*, 647.
[25] Q. He, S.-X. L. Luo, T. Jin, M. Liu, S. Park, A. Alexander-Katz, B. R. Mcdonald, F. Fornasiero, T. M. Swager, *Chem. Mater.* **2023**, *35*, 1674.
[26] V. G. Snider, C. L. Hill, *J. Hazard. Mater.* **2023**, *442*, 130015.
[27] J. Haldar, D. An, L. Álvarez De Cienfuegos, J. Chen, A. M. Klibanov, *Proc. Natl. Acad. Sci. U. S. A.* **2006**, *103*, 17667.
[28] K. G. Neoh, E. T. Kang, *ACS Appl. Mater. Interfaces* **2011**, *3*, 2808.
[29] J. Hoque, S. Ghosh, K. Paramanandham, J. Haldar, *ACS Appl. Mater. Interfaces* **2019**, *11*, 39150.
[30] M. K. L. N. Sikosana, A. Ruland, C. Werner, L. D. Renner, *Appl. Environ. Microbiol.* **2022**, *88*, e02241.
[31] M. R. Nejadnik, H. C. Van Der Mei, W. Norde, H. J. Busscher, *Biomaterials* **2008**, *29*, 4117.
[32] X. Chu, F. Yang, H. Tang, *Chin. J. Chem.* **2022**, *40*, 2988.
[33] A. Conde, A. Durán, J. J. de Damborenea, *Prog. Org. Coat.* **2003**, *46*, 288.
[34] U. Riaz, C. Nwaoha, S. M. Ashraf, *Prog. Org. Coat.* **2014**, *77*, 743.
[35] M. J. Palimi, E. Alibakhshi, B. Ramezanzadeh, G. Bahlakeh, M. Mahdavian, *J. Taiwan Inst. Chem. Eng.* **2018**, *82*, 261.
[36] M. Ates, *J. Adhes. Sci. Technol.* **2016**, *30*, 1510.
[37] T. Ohtsuka, *Int. J. Corros.* **2012**, *2012*, 915090.
[38] S. Lin, H. Shih, F. Mansfeld, *Corros. Sci.* **1992**, *33*, 1331.
[39] M. Stratmann, R. Feser, A. Leng, *Electrochim. Acta* **1994**, *39*, 1207.
[40] N. Lavielle, D. Asker, B. D. Hatton, *Soft Matter* **2021**, *17*, 936.
[41] A. L. Patterson, B. Wenning, G. Rizis, D. R. Calabrese, J. A. Finlay, S. C. Franco, R. N. Zuckermann, A. S. Clare, E. J. Kramer, C. K. Ober, R. A. Segalman, *Macromolecules* **2017**, *50*, 2656.
[42] D. R. Calabrese, B. Wenning, J. A. Finlay, M. E. Callow, J. A. Callow, D. Fischer, C. K. Ober, *Polym. Adv. Technol.* **2015**, *26*, 829.
[43] A. K. Leonardi, R. Medhi, A. Zhang, N. Düzen, J. A. Finlay, J. L. Clarke, A. S. Clare, C. K. Ober, *Biomacromolecules* **2022**, *23*, 2697.
[44] S. A. Stern, V. M. Shah, B. J. Hardy, *J. Polym. Sci., Part B: Polym. Phys.* **1987**, *25*, 1263.
[45] H. Zhang, A. Cloud, in Fall Technical Conference, Global Advances in Materials and Process Engineering, SAMPE, Dallas, TX, **2006**, pp. 72.
[46] R. L. Mickelsen, R. C. Hall, *Am. Ind. Hyg. Assoc. J.* **1987**, *48*, 941.
[47] J. R. Williams, *Am. Ind. Hyg. Assoc. J.* **1979**, *40*, 877.
[48] M.-J. Chen, L.i-H. Cheng, T.-P. Tseng, Y.-S. Huang, C.-H.o Lin, C.-H. Lai, *Eur. Polym. J.* **2015**, *66*, 407.
[49] L.i-H. Cheng, M.-J. Chen, W.-H. Cheng, C.-H.o Lin, C.-H. Lai, *J. Memb. Sci.* **2012**, *409–410*, 180.
[50] M. Métayer, M. Labbé, S. Marais, D. Langevin, C. Chappey, F. Dreux, M. Brainville, P. Belliard, *Polym. Test.* **1999**, *18*, 533.

[51] A. K. Ekenseair, **2010**.
[52] T.-H. Yang, S. J. Lue, *J. Macromol. Sci., Part B: Phys.* **2013**, *52*, 1009.
[53] M. B. Wisnudel, J. M. Torkelson, *Macromolecules* **1996**, *29*, 6193.
[54] M. J. Varady, D. A. Boyne, T. P. Pearl, R. H. Lambeth, B. A. Mantooth, *Polymer* **2019**, *180*, 121697.
[55] V. S. Shirure, S. C. George, *Lab Chip* **2017**, *17*, 681.
[56] T. T. Ngo, C. L. Liotta, C. A. Eckert, S. G. Kazarian, *J. Supercrit. Fluids* **2003**, *27*, 215.
[57] F. Donati, A. Pucci, G. Ruggeri, *Phys. Chem. Chem. Phys.* **2009**, *11*, 6276.
[58] A. V. Nair, W. Yanhong, T. G. Paunescu, R. Bouley, D. Brown, *PLoS One* **2019**, *14*, e0219940.
[59] S. R. Kwon, P. W. Wertz, Y. Li, D. C. N. Chan, *Int. J. Cosmet. Sci.* **2012**, *34*, 97.
[60] D. Solpan, S. Duran, D. Saraydin, O. Güven, *Radiat. Phys. Chem.* **2003**, *66*, 117.
[61] T. E. Shearmur, D. W. Drew, A. S. Clough, M. G. D. Van Der Grinten, A. T. Slark, *Polymer* **1996**, *37*, 2695.
[62] J. Slootman, C. J. Yeh, P. Millereau, J. Comtet, C. Creton, *Proc. Natl. Acad. Sci. U. S. A.* **2022**, *119*, e2116127119.
[63] M. L. Rencheck, B. T. Mackey, Y.u-Y. Hu, C.-C. Chang, M. D. Sangid, C. S. Davis, *Adv. Eng. Mater.* **2022**, *24*, 2101080.
[64] M. Hai, Q. Zhang, Z. Li, M. Cheng, A. J. C. Kuehne, F. Shi, *Supramol. Mater.* **2022**, *1*, 100009.
[65] M. Adiraj Iyer, D. T. Eddington, *Lab Chip* **2019**, *19*, 574.
[66] H. Tong, Q. Jiang, X. Zhong, X. Hu, *Environ. Sci. Pollut. Res.* **2021**, *28*, 4209.
[67] N. Bosq, N. Guigo, J. Persello, N. Sbirrazzuoli, *Phys. Chem. Chem. Phys.* **2014**, *16*, 7830.
[68] J. Rieger, *J. Therm. Anal.* **1996**, *46*, 965.
[69] F. L. Arbeloa, P. R. Ojeda, I. L. Arbeloa, *J. Lumin.* **1989**, *44*, 105.
[70] G. Yeroslavsky, M. Kamimura, R. Inoue, Y. Kogo, K. Soga, *J. Photopolym. Sci. Technol.* **2018**, *31*, 533.
[71] X. M. Han, J. Lin, R. B. Xing, J. Fu, S. B. Wang, *Mater. Lett.* **2003**, *57*, 1355.
[72] F. A. Gotch, J. A. Sargent, M. L. Keen, *Kidney Int.* **2000**, *58*, S3.
[73] F. Gotch, *Nephrol., Dial., Transplant.* **1998**, *13*, 10.
[74] X. Chen, J. A. Gardella, P. L. Kumler, *Macromolecules* **1992**, *25*, 6631.
[75] B. M. D. O'driscoll, R. A. Kelly, M. Shaw, P. Mokarian-Tabari, G. Liontos, K. Ntetsikas, A. Avgeropoulos, N. Petkov, M. A. Morris, *Eur. Polym. J.* **2013**, *49*, 3445.
[76] A. Leonardi, A. C. Zhang, N. Düzen, N. Aldred, J. A. Finlay, J. L. Clarke, A. S. Clare, R. A. Segalman, C. K. Ober, *ACS Appl. Mater. Interfaces* **2021**, *13*, 28790.